

Observation of sidearm splitting studied by high resolution X-ray radiography

Shevchenko, N.; Grenzer, J.; Keplinger, O.; Rack, A.; Eckert, S.;

Originally published:

January 2020

International Journal of Materials Research 111(2020)1, 11-16

DOI: <https://doi.org/10.3139/146.111835>

Perma-Link to Publication Repository of HZDR:

<https://www.hzdr.de/publications/Publ-28827>

Release of the secondary publication
on the basis of the German Copyright Law § 38 Section 4.

Zeitschrift für Metallkunde: International Journal of Materials Research

Observation of sidearm splitting studied by high resolution X-ray radiography

--Manuscript Draft--

Manuscript Number:	
Full Title:	Observation of sidearm splitting studied by high resolution X-ray radiography
Article Type:	Original Paper
Section/Category:	MSE2018
Keywords:	Dendritic growth; Solidification; Sidearm splitting; Synchrotron X-ray imaging
Corresponding Author:	Natalia Shevchenko Helmholtz-Zentrum Dresden-Rossendorf Dresden, Sachsen GERMANY
Corresponding Author Secondary Information:	
Corresponding Author's Institution:	Helmholtz-Zentrum Dresden-Rossendorf
Corresponding Author's Secondary Institution:	
First Author:	Natalia Shevchenko
First Author Secondary Information:	
Order of Authors:	Natalia Shevchenko Joerg Grenzer Olga Keplinger Alexander Rack Sven Eckert
Order of Authors Secondary Information:	
Manuscript Region of Origin:	GERMANY
Abstract:	The local dynamics of dendritic sidearms during the growth stage are studied by in-situ radiography observations at high spatial resolution of $< 1 \mu\text{m}$. A flat sample of a Ga-In alloy is solidified top-down applying a vertical temperature gradient. The evolving dendritic microstructure is visualized using synchrotron X-ray imaging at the beamline ID19 (ESRF, France). The experimental investigations on the dendrite evolution revealed a transition from a four-fold symmetry to a hyperbranched dendritic morphology. Both, the sidearm-splitting phenomena – responsible for this morphological transition – as well as the arm growth dynamics are characterized by image processing.
Suggested Reviewers:	Wajira Mirihanage, Dr. University of Manchester wajira.mirihanage@manchester.ac.uk Nathalie Mangelinck-Noel, Dr. CNRS nathalie.mangelinck@im2np.fr Biao Cai, Dr. University of Birmingham B.Cai@bham.ac.uk
Author Comments:	

Observation of sidearm splitting studied by high resolution X-ray radiography

Natalia Shevchenko^a, Joerg Grenzer^a, Olga Keplinger^a, Alexander Rack^b, Sven Eckert^a

^a Helmholtz-Zentrum Dresden-Rossendorf, Dresden, Germany

^b ESRF – The European Synchrotron, Grenoble, France

Abstract: The local dynamics of dendritic sidearms during the growth stage are studied by in-situ radiography observations at high spatial resolution of $< 1 \mu\text{m}$. A flat sample of a Ga-In alloy is solidified top-down applying a vertical temperature gradient. The evolving dendritic microstructure is visualized using synchrotron X-ray imaging at the beamline ID19 (ESRF, France). The experimental investigations on the dendrite evolution revealed a transition from a four-fold symmetry to a hyperbranched dendritic morphology. Both, the sidearm-splitting phenomena – responsible for this morphological transition – as well as the arm growth dynamics are characterized by image processing.

Keywords: Dendritic growth, Solidification, Sidearm splitting, Synchrotron X-ray imaging

1. Introduction

The dendrite growth kinetics and morphology are gaining increasing interest in the solidification science and casting industry. Recently, high speed synchrotron tomography has been applied to study solidification processes, including dendritic growth [1-3], solid phase coarsening [4-5], the evolution of equiaxed dendrites [6] and intermetallic phase formation [7]. This technique allows in-situ studies of the three-dimensional (3D) structure of growing dendrites and, in particular, their side-branch morphology. The side-branch morphology is intimately related to the properties of the solidifying structure and to the resulting microsegregation process. Detailed analyses of the growing dendrites in Al – Cu alloys revealed complicated 3D structures of the sidearm morphology [1, 3]. Unlike cylindrical secondary arms in transparent organic materials [8, 9], which are commonly used as metal analogues, the Al dendrite sidearms have shown an almost plate-like form [1] or a dense-branched coralline-like (seaweed) morphology [3]. A morphological instability of a flat secondary arm leads to multiple tertiary side branches and split tips [1]. Tip splitting of primary dendrites and the occurrence of seaweed microstructures has been widely studied in thin cells imaged via 2D in-situ methods in transparent systems [10-12] and metallic alloys [13]. Seaweed morphology in transparent materials is believed to be related to the low anisotropy of the solid–liquid interface energy because the growth process is then not constrained to some specific orientation [12].

The importance of the anisotropy for the evolution of dendritic morphology has long been known [14, 15]. It was shown that any small anisotropy can be described by two independent parameters ϵ_1 and ϵ_2 , which parametrize the strength of the four- and six-fold anisotropy cubic-harmonic functions [14]. Phase-field simulations have established that dendrite growth

1 along the commonly observed $\langle 100 \rangle$ crystallographic directions is stable for large values of
2 ϵ_1 , while negative large values of ϵ_2 tend to support $\langle 110 \rangle$ growth, with a domain of
3
4 “hyperbranched” structures in between. It has been shown, that just a small misorientation (a
5
6 few degrees) between the principal $\langle 100 \rangle$ crystal axes and growth directions of these planes
7
8 can induce hyperbranched dendrite structure [14, 15]. The possibility of altering anisotropy
9
10 parameters by the addition of solute elements have been experimentally and computationally
11
12 demonstrated [14]. Further work and advanced techniques are needed to clarify the influence
13
14 of other factors (melt flow, magnetic field) on dendritic arm morphology.
15
16

17 Radiography as a 2D imaging method provides dynamical data of high temporal and spatial
18
19 resolution at a low noise level. Tomography has a much lower temporal resolution, but,
20
21 allows for obtaining 3D spatial information about the morphology and provides very accurate
22
23 3D images about the evolution of the dendritic sidearm structure itself. But, a fast revolution
24
25 of a melted sample on a tomography stage may induce additional effects on the
26
27 microstructure. Exploiting, however, X-ray transmission contrast differences 2D synchrotron
28
29 radiography data can be processed and analyzed to retrieve three-dimensional (3D) spatial
30
31 information on growing dendrites from X-ray transmission contrast differences [16]. The
32
33 ability to carry out a 3D reconstruction of microstructure details involves the consideration of
34
35 variations in the solute-composition in the liquid and thickness variations in the growing
36
37 dendrites [16]. Based on the high spatial and temporal resolution and advanced data
38
39 processing, synchrotron radiography of a thin sample is a highly suitable experimental
40
41 technique for studying the interface dynamics of dendritic structures in metallic alloys under
42
43 well-defined conditions [16 - 18].
44
45
46
47
48
49
50
51
52

53 In this work, we report on recent high-resolution synchrotron experiments using a Ga-In alloy
54
55 in which the dendrite sidearm evolution and the phenomenon of sidearm splitting are
56
57
58
59
60
61
62
63
64
65

observed in-situ. The paper is focused on morphological transitions such as the evolution from four-fold symmetric dendrites to hyperbranched dendritic structures.

2. Experimental setup and data processing

In-situ solidification studies of metallic systems have been performed using low melting temperature Gallium - Indium alloys, a model system, studying the growth of Indium dendrites in Ga enriched melt [19 - 21]. These alloys provide an excellent attenuation contrast between the indium crystals and the liquid phase. Ga – In alloys were chosen because they have similar thermo-physical properties like steel or other industrial relevant alloys, but, the near-eutectic compositions are liquid at room temperature and, therefore, are much easier to handle.

The visualization experiments were performed at the ID19 beamline at the ESRF (Grenoble). The solidification setup (Fig. 1) was already employed in previous radiographic investigations carried out by means of a microfocus X-ray tube and was described in detail elsewhere [19, 20].

The nominal composition of the Ga - 35 wt% In alloys were prepared from 99.99% Ga and 99.99% In. The alloy was melted and filled into a windowed Hele-Shaw cell with a liquid metal volume of $22 \times 22 \times 0.2 \text{ mm}^3$.

Two pairs of Peltier elements are mounted on the top and bottom edges of the flat solidification cell. One pair of Peltier elements was used as a heater or as a cooler depending on the purposed upward or downward directions of solidification. The synchronized regulation of the power of both Peltier elements by means of a PID controller unit allowed for the adjustment of the cooling rate and the temperature gradient during the process. The distance between the heater and the cooler was $\sim 23 \text{ mm}$. The temperature difference ΔT

between the heater and the cooler is measured using two miniature K-type thermocouples, which have a thermal contact to the outer surface of the cell near the edge of Peltier elements. The accuracy of the temperature control is ± 0.2 K. The vertical temperature gradient was calculated from the temperature difference measured between these two thermocouples. In the present experiments, cooling rates of 0.002 K/s and a temperature gradient of ~ 2 K/mm were applied.

The solidification sample was exposed to a monochromatic, parallel X-ray beam with an X-ray photon energy of 40 keV. Conventional transmission radiographs were obtained by means of a scintillator that provides a spatial sampling of $< 1 \mu\text{m}$ and which was coupled with a high speed sCMOS camera (PCO.edge) with 2048×2048 pixels (effective pixel size of nominal $0.65 \mu\text{m}$). This equipment leads to a field of view of about $1.3 \times 1.3 \text{ mm}^2$ [22]. The distance between the detector and sample was kept constant at ~ 10 cm. A single radiogram was acquired at exposure times of 0.5 seconds. In order to change the location of the observation window, the position of the solidification cell was manipulated with respect to the X-ray beam by a motorized positioning system with a minimum translation step of $10 \mu\text{m}$.

Series of experiments were realized applying multiple cycles of solidification and remelting processes. Before each experiment the Ga-In alloy was heated to a temperature of 80°C and for a time period of a few minutes. During this stage the sample was controlled by real-time radiography to ensure that the alloy was homogeneously mixed before the cooling process was started. After recording reference images of the completely molten alloy, the cooling of the melt and the image acquisition were initiated. Dark field images and flat field images were also recorded for further data processing.

As a first step in the image processing, the dark image of the camera was subtracted from all frames. A flat field correction was performed by first selecting a reference frame of the

observation window in the fully liquid state, and then using a smoothed version of this frame. The quantitative evaluation of geometrical features of individual dendrites and its sidebranches was performed using ImageJ and MatLab scripts. The dendrite tip velocity was calculated by tracking the individual dendrite tips using ImageJ, and then averaging the individual dendrite velocities.

3. Results and discussion

The Ga–In alloy was solidified in vertical direction starting from the top of the solidification cell at a controlled cooling rate of 0.002 K/s and at a temperature gradient of ~2 K/mm. Figure 2 contains radiographs illustrating the growth process of dendrites and its morphology at different growth stages; the corresponding temperature evolution is shown in Figure 3. The first dendrites are observed at the bottom edge of the Peltier cooler at a temperature of ~30 °C and about 3000 s after the start of the experiment. Figure 2(a) shows primary Indium crystals emerging at the top left corner of the observation window, which are not aligned with the direction of the temperature gradient. The angle between the gravity vector and the dendrite growth direction was approx. 55°. The growing dendrites have a typical dendrite-like form with an angle of ~90° between the primary trunk and sidearm directions, indicating a growth along principal crystallographic axes. Indium dendrites with a BCT (body-centred tetragonal) crystal structure may grow along <001> direction with a four-fold symmetry of secondary arms*. The local conditions (temperature, solute concentration, melt flow) may suppress the development of some side arms. In our case, the sidearms only grow on one side of dendrite trunk, which results from the orientation of the arm with respect to the positive vertical temperature gradient.

1
2
3
4
5
6
7
8
9
10
11
12
13
14
15
16
17
18
19
20
21
22
23
24
25
26
27
28
29
30
31
32
33
34
35
36
37
38
39
40
41
42
43
44
45
46
47
48
49
50
51
52
53
54
55
56
57
58
59
60
61
62
63
64
65

[[*Comment for footnote: For example, in metals with FCC (face-centred cubic) crystal structure the growth direction of dendrites corresponds to $\langle 100 \rangle$ principal crystallographic axes [23]. BCT crystal structure of Indium can be easily extrapolated by FCC crystal structure with a lattice parameter corresponding to the c-axis of the BCT. In this case the $\langle 001 \rangle$ BCT growth direction will correspond to the $\langle 100 \rangle$ FCC growth direction. For simplification, we refer in the further text to the FCC crystal structure. This means that the primary and side arms are growing in the $\langle 100 \rangle$ FCC directions with the four-fold symmetry of secondary arms.]]

During the early solidification stage an average tip velocity of $\sim 13 \mu\text{m/s}$ was measured in the region close to the Peltier cooler (Fig. 3). The fast growth of the dendrites is associated with a needle-like form of both, the primary dendrite tip and the side arms (Fig. 2(a)). In the further course of the process, the average tip velocity decreases from $13 \mu\text{m/s}$ to $0.2 \mu\text{m/s}$ over a transient period of 1000 seconds. Figure 2(b) shows clearly a significant change of the microstructure during the deceleration stage of the dendrite growth. During this time a continuous coarsening of the dendrite structure takes place resulting in an increase of the secondary spacing λ_2 from approximately $10 \mu\text{m}$ at the beginning of the deceleration stage to a mean value of $25 \mu\text{m}$ at $t \sim 1000 \text{ s}$ and in an increase of the tip radius up to $\sim 5 \mu\text{m}$. After deceleration the dendrite tip velocities show only small fluctuations around a value of $\sim 0.2 \mu\text{m/s}$. Further dendrite coarsening is observed during the slow steady growth stage (Fig. 2 (c)).

With decreasing tip velocity the angle between the gravity vector and a dendrite growth direction changes from $\sim 55^\circ$ to $\sim 49^\circ$. This indicates a misorientation angle between the growth direction and the initial growth direction of approximately 6° . The growth direction of dendrites might be rearranged toward the thermal gradient direction as the growth velocity is

decreased [11]. In addition to this, one observes dramatic changes of dendrite morphology, especially the evolution of new secondary branches (Fig. 2(d)). These dendrites reveal a so-called ‘hyperbranched’ structure and have obviously more than 4 secondary arms. Note that, this observation window is restricted to four dendrites. All dendrites in this grain (more than 10 dendrites) reveal a similar morphological evolution to the hyperbranched structure.

For studying the temporal evolution of the sidearm morphology during the slow growth stage we selected an image section of 200 x 200 μm located near a dendrite tip. Figure 4(a)-(d) present four X-ray images acquired at different time steps showing one segment of one specific dendrite. The radiography doesn’t allow us to obtain any 3D spatial information about the morphology of the dendritic sidearms. However, a geometrical analysis could provide a simple reconstruction of the morphology of the sidearms. The projections of the sidearms which are perpendicular to the sample plane (top view) show an elliptical shape at early solidification stages. At first, the fitting of the projection by an ellipse was performed. Then, calculations of a shortest diameter and a longest diameter of the elliptical projection were done for four sidearms near the tip as shown in Fig. 5(a).

Figures 4(a)-(b) demonstrate an example of shape evolution of individual arms. The longest diameter (D_{max}) of the elliptical projection increases from 20 to $\sim 38 \mu\text{m}$ for the time period up to approximately 1700 s (Fig. 5(b)). At the same time, the relation of a shortest diameter to a longest diameter ($D_{\text{min}}/D_{\text{max}}$) of the elliptical projection decreases from approx. 0.5 to 0.38. Such geometrical parameter changes indicate that nearly cylindrical sidearms transform to a flat arm, so called plate-like form as in ref [1]. The radiograph in Fig. 4(d) shows that the projections of the sidearms change from an ellipse (1) to two overlapping ellipses (2). Very likely, this variation of the projection area is associated with the splitting of the side arm tip as suggested by the schematic view in Fig. 5(a). As solidification advances, the arm continues to

grow, forming two side arms from the perturbations (Fig. 4(c) and (d)). For example, the sidearm 3 in Fig. 4(d) divides into two parts, indicating a splitted pattern. This arm splitting effect results in a drop in the geometrical parameters after 1700 s presented in the Fig. 5(b).

Note that, the splitting of the side arms can be detected to occur in a close vicinity to the dendrite tip. Here, the dimensions of the dendrite structure are still so small that no dominant influence of the sidewalls on the phenomenon is to be expected.

Several factors could be the origin of the sidearm splitting phenomenon. As can be seen from the figure 4, the shape of sidearm changed during the experiment. The tip radius of the arm increases while the arm grows. Finally, the top interface breaks up and splits into two new branches. Y. Chen et al [13] demonstrated that the shape of the dendrite tip in the seaweed regime undergoes a similar transition process. Phase-field simulations show that the tip splitting is caused by the Mullins–Sekerka instability occurring when the cell/dendrite tip becomes too wide [13]. The same mechanism involving Mullins-Sekerka morphological instability at the solid-liquid interface determinates the transition from a planar front to a cellular front and then to dendritic growth [24].

Crystalline anisotropy can have a significant effect on the morphology of the solid-liquid interface and, hence, on the arm morphology. In the current experiment, the crystalline anisotropy could stem from both, the variation of the solute concentration as well as an angle between the temperature gradient and the growth direction. The solute concentration at the solidification front and within mushy zone could vary during the solidification process [19]. A more detailed analysis of these particular processes is the subject of the ongoing work.

4. Summary

1 This work presents in-situ observations of the transition from the classical four-fold
2 symmetric dendrites to the hyperbranched dendritic morphology in the model Ga – 35%In
3 alloy. A morphological transition involving the splitting of dendrite sidearms has been
4 detected at a cooling rate of 0.002 K/s and a vertical temperature gradient of ~2 K/mm. Under
5 the given experimental conditions the high temporal and spatial resolution of X-ray
6 visualization allowed us to characterize both the sidearm morphology evolution as well as the
7 sidearm splitting phenomenon. Based on the preliminary results obtained in this work using
8 the high-resolution synchrotron radiography, advanced data processing can be carried out as a
9 next step to provide useful data for validation of numerical simulations.
10
11
12
13
14
15
16
17
18
19
20
21
22
23

24 **Acknowledgements**

25
26 The authors gratefully acknowledge the scientific and technical support at the Beamline ID19
27 at ESRF (Grenoble, France), especially Dr. Valentina Cantelli and Jean-Paul Valade and we
28 thank the Department of Research Technology at HZDR for the continuing support during the
29 preparation of the experiment.
30
31
32
33
34
35
36
37
38

39 **References**

- 40
41 [1] J.W. Gibbs, K.A. Mohan, E.B. Gulsoy, A.J. Shahani, X. Xiao, C.A. Bouman, M. De
42 Graef, P.W. Voorhees: Sci. Rep. 5 (2015) 11824. DOI: 10.1038/srep11824.
43
44 [2] O. Ludwig, M. Dimichiel, L.U.C. Salvo, M. Su ery, P. Falus, In-situ three-dimensional
45 microstructural investigation of solidification of an Al-Cu alloy by ultrafast X-ray
46 microtomography, Metall. Mater. Trans. A 36 (2005) 1515-1523.
47
48 [3] B. Cai, J. Wang, A. Kao, K. Pericleous, A.B. Phillion, R.C. Atwood, P.D. Lee: Acta
49 Mater. 117 (2016) 160-169. DOI: 10.1016/j.actamat.2016.07.002
50
51
52
53
54
55
56
57
58
59
60
61
62
63
64
65

- [4] N. Limodin, L. Salvo, E. Boller, M. Suery, M. Felberbaum, S. Gaillieue, K. Madi: *Acta Mater.* 57 (2009) 2300. DOI:10.1016/j.actamat.2009.01.035
- [5] L.K. Aagesen, J.L. Fife, E.M. Lauridsen, P.W. Voorhees: *Scr. Mater.* 64 (2011) 394. DOI: 10.1016/j.scriptamat.2010.10.040
- [6] S. Shuai, E. Guo, A.B. Phillion, M. D. Callaghan, T. Jing, P. D. Lee: *Acta Materialia* 118 (2016) 260-269. DOI: 10.1016/j.actamat.2016.07.047
- [7] J. M. Yu, N. Wanderka, A. Rack, R. Daudin, E. Boller, H. Markötter, A. Manzoni, F. Vogel, T. Arlt, I. Manke, J. Banhart: *Acta Materialia* 129 (2017) 194. DOI: 10.1016/j.actamat.2017.02.048
- [8] S.-C. Huang, M. E. Glicksman: *Acta Metall.* 29, 717–734 (1981). DOI: 10.1016/0001-6160(81)90116-4
- [9] S. Liu, S.Z. Lu, A. Hellawell: *Journal of Crystal Growth* 234 (2002) 751. DOI: 10.1016/S0022-0248(01)01680-3
- [10] S. Akamatsu, G. Faivre, T. Ihle: *Phys. Rev. E* 51 (1995) 4751. DOI: 10.1103/PhysRevE.51.4751
- [11] A. Pocheau, J. Deschamps, M. Georgelin: *JOM* 59 (2007) 71-76. DOI: 10.1007/s11837-007-0093-5
- [12] B. Utter, E. Bodenschatz: *Physical Review E* 66 (2002), 051604. DOI: 10.1103/PhysRevE.66.051604
- [13] Y. Chen, B. Billia, D.Z. Li, H. Nguyen-Thi, N.M. Xiao, A.A. Bogno: *Acta Mater* 66 (2014) 219. DOI: 10.1016/j.actamat.2013.11.069
- [14] T. Haxhimali, A. Karma, F. Gonzales, M. Rappaz: *Nat. Mat* 5 (8) (2006) 660. DOI: 10.1038/nmat1693

- [15] M. Asta, C. Beckermann, A. Karma, W. Kurz, R. Napolitano, M. Plapp, G. Purdy, M. Rappaz, R. Trivedi: *Acta Mater.* 57 (2009) 941. DOI: 10.1016/j.actamat.2008.10.020
- [16] W.U. Mirihanage, K. V. Falch, I. Snigireva, A. Snigirev, Y. J. Li, L. Arnberg, R. H. Mathiesen: *Acta Mater.* 81 (2014) 241. DOI: 10.1016/j.actamat.2014.08.016
- [17] H. Neumann-Heyme, N. Shevchenko, Z. Lei, K. Eckert, O. Keplinger, J. Grenzer, C. Beckermann, S. Eckert: *Acta Mater.* 146 (2018) 176. DOI: 10.1016/j.actamat.2017.12.056
- [18] R.H. Mathiesen, L. Arnberg: *Acta Mater.* 53 (2005) 947. DOI: 10.1016/j.actamat.2004.10.050
- [19] N. Shevchenko, O. Roshchupkina, O. Sokolova, S. Eckert: *Journal of Crystal Growth* 417 (2015) 1. DOI: 10.1016/j.jcrysgro.2014.11.043
- [20] N. Shevchenko, S. Boden, G. Gerbeth, S. Eckert: *Metall. Mater. Trans. A* 44 (8) (2013) 3797. DOI: 10.1007/s11661-013-1711-1
- [21] S. Karagadde, L. Yuan, N. Shevchenko, S. Eckert, P.D. Lee: *Acta Materialia* 79 (2014) 168. DOI: 10.1016/j.actamat.2014.07.002
- [22] P.-A. Douissard, A. Cecilia, X. Rochet, X. Chapel, T. Martin, T. van de Kamp, L. Helfen, T. Baumbach, L. Luquot, X. Xiao, J. Meinhardt, A. Rack: *Journal of Instrumentation* 7 (2012) P09016. DOI: 10.1088/1748-0221/7/09/P09016
- [23] J.A. Dantzig, M. Rappaz: *Solidification*, EFPL Press, 2009.
- [24] W.W. Mullins, R.F. Sekerka: *Stability of a planar interface during solidification of a dilute binary alloy*, *J. Appl. Phys.* 35 (1964) 444. DOI: 10.1063/1.1713333

List of figure captions

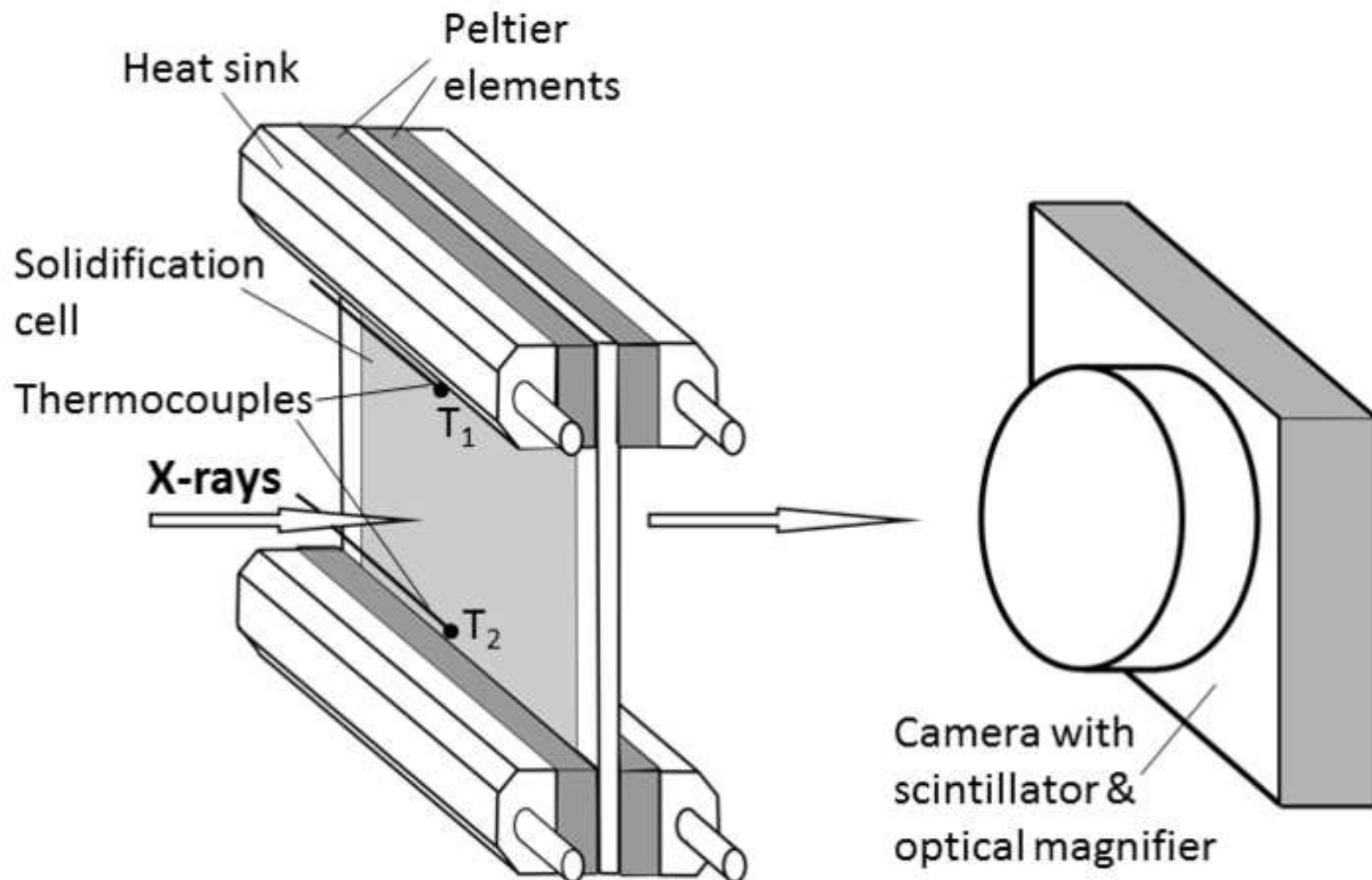
Figure 1: Schematic of the experimental setup with a flat solidification cell.

Figure 2: Snapshots of the solidifying dendritic structure in Ga - 35wt%In alloys captured at different time: a) 55 s, b) 870 s, c) 2090 s, d) 8825 s; ($t = 0$ corresponds to the appearance of the first dendrite near the Peltier cooler).

Figure 3: Tip velocity (left scale) averaged for four selected dendrites, which are shown in Fig. 2(a-c) ($t = 0$ corresponds to the appearance of the first dendrite near the Peltier cooler). Thermal regime (right scale): a line T_1 – temperature curve near the cooler; a line T_2 – temperature curve near the heater. The thermocouples T_1 and T_2 were positioned at the edge of the Peltier cooler and heater, respectively.

Figure 4: Sequence of X-ray images showing the development of secondary dendrite arms at different time: (a) 740 s, (b) 1670 s, (c) 3179 s and (d) 8825 s, [side arms with typical shapes are labelled in (d)].

Figure 5: (a) Definition of ellipses during the different stages of the growth and the geometrical parameters D_{\max} and D_{\min} ; (b) Evolution of geometrical parameters (D_{\max} and D_{\min}) of the perpendicular sidearms (from arms 1 to arms 2), which are explained in the schematic view (a).



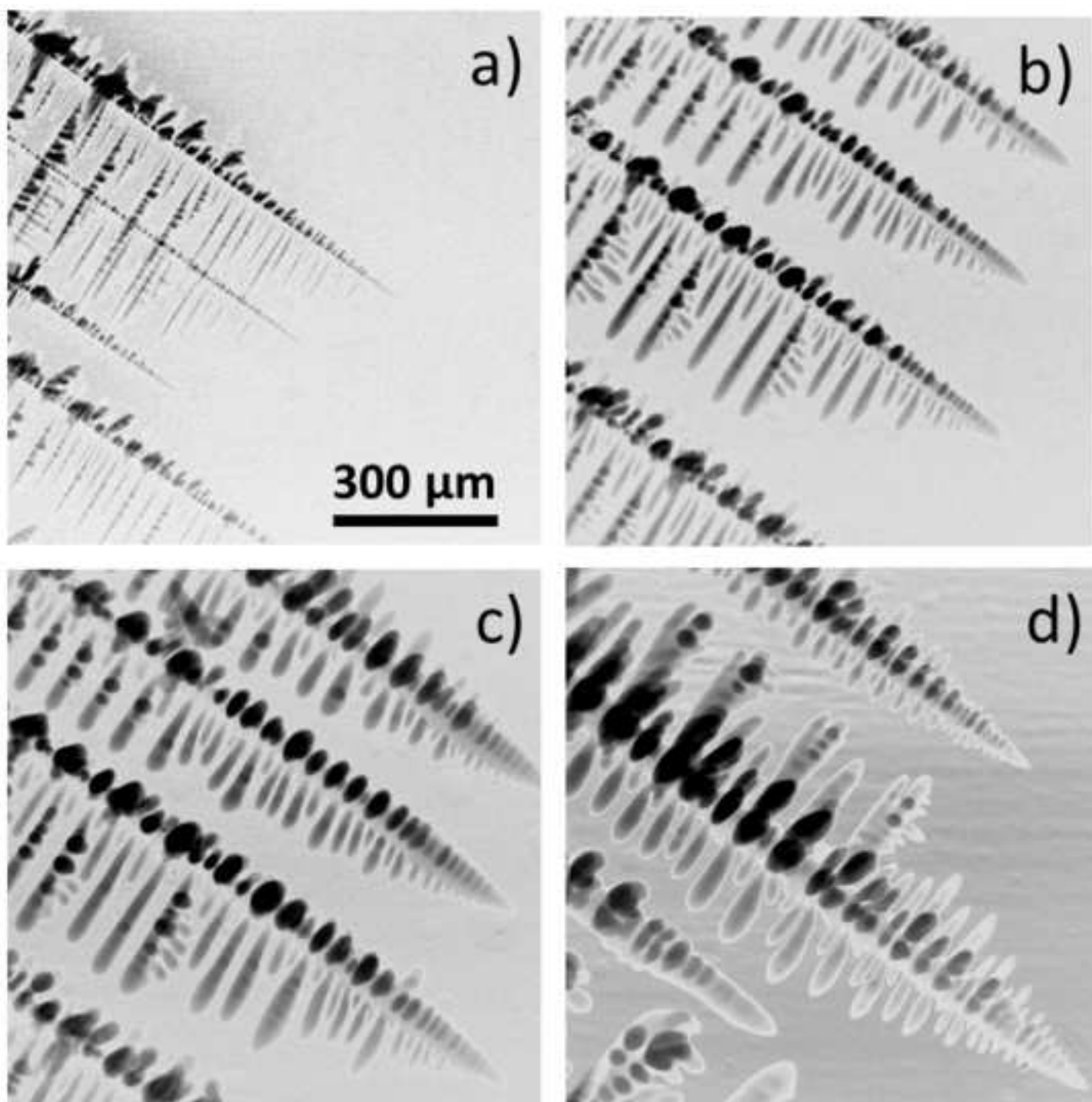


Figure3

